

Anomalous Self-Energy Effects of the B_{1g} Phonon in $Y_{1-x}(\text{Pr}, \text{Ca})_x\text{Ba}_2\text{Cu}_3\text{O}_7$ Films

A. Bock, S. Ostertun, R. Das Sharma, M. Rübhausen,* and K.-O. Subke
*Institut für Angewandte Physik und Zentrum für Mikrostrukturforschung,
 Universität Hamburg, Jungiusstraße 11, D-20355 Hamburg, Germany*

C.T. Rieck

*I. Institut für Theoretische Physik, Universität Hamburg, Jungiusstraße 9, D-20355 Hamburg,
 Germany*

(June 24, 2018)

Abstract

In Raman spectra of cuprate superconductors the gap shows up both directly, via a redistribution of the electronic background, the so-called “ 2Δ peaks”, and indirectly, e.g. via the renormalization of phononic excitations. We use a model that allows us to study the redistribution and the related phonon self-energy effects simultaneously. We apply this model to the B_{1g} phonon of $Y_{1-x}(\text{Pr}, \text{Ca})_x\text{Ba}_2\text{Cu}_3\text{O}_7$ films, where Pr or Ca substitution enables us to investigate under- and overdoped samples. While various self-energy effects can be explained by the strength and energy of the 2Δ peaks, anomalies remain. We discuss possible origins of these anomalies.

PACS numbers: 74.25.Gz, 74.62.Dh, 74.72.Bk, 74.76.Bz, 78.30.Er

I. INTRODUCTION

Some phonons in high-temperature superconductors show remarkable self-energy effects when the superconducting gap Δ opens. The strongest effects so far have been observed for modes originating from the copper oxygen planes,¹ in which the pairing mechanism is believed to be located. One example is the B_{1g} phonon at 340 cm^{-1} in RE-123 compounds (RE: rare earth or Y) where renormalizations have been observed in neutron² as well as in Raman experiments.³ In the latter the B_{1g} phonon has a Fano-type line shape as a consequence of the fact, that some of the excitations which renormalize it are also Raman-active.⁴ This holds above T_c where quasi-particle scattering leads to a structureless incoherent background⁵ as well as below T_c when the background redistributes and pair-breaking excitations become observable. Considerable theoretical works have been carried out to describe the redistribution which leads to the development of so-called “ 2Δ peaks”.^{6–8} The main features which are observed in the spectra seem to favor a d -wave gap, however, not all details are understood at present.⁹ For example the fact that the redistribution in B_{1g} symmetry weakens with decreasing doping¹⁰ indicates that vertex corrections due to strong correlations may play a considerable role, as e.g. angle-resolved photoemission spectroscopy (ARPES) shows well-defined quasi-particle peaks down to low doping levels below T_c .¹¹

In this work we investigate the renormalization of the B_{1g} phonon and the redistributed background in $Y_{1-x}(\text{Pr}, \text{Ca})_x\text{Ba}_2\text{Cu}_3\text{O}_7$ films which exhibit B_{1g} 2Δ peaks at low temperatures above, near, and below the phonon frequency. Our aims are first to identify the shape of the electronic background in the presence of strongly interacting phonons in order to provide substantial data for theoretical descriptions, and second to correlate the redistribution and the self-energy effects, thereby allowing of an investigation of the strength of the electron-phonon coupling. So far, simultaneous descriptions of the B_{1g} phonon and the interacting background have been obtained in a microscopic approach by Devereaux *et al.*¹² and a phenomenological one by Chen *et al.*¹³ Being mainly interested in the electronic contribution, the latter authors have taken only a frequency-dependent imaginary part of the electronic response function into account, treating the real part as constant. As we are interested in the phonon self-energies as well, this approximation is not justified here. The microscopic description considers the full frequency-dependent electronic response and provides a basis for the interpretation of the fit parameters. We will briefly recall that model and show how non-resonant phonon Raman scattering, which is to some extent observed in case of the B_{1g} phonon,¹⁴ can be described via a correction of the electron-photon vertex. We then connect the obtained result to the phenomenological Fano formula of Chen *et al.*¹³ by including a resonant excitation channel for the phonon.

The important improvement of our approach is a phenomenological description of the frequency-dependent real and imaginary parts of the electronic response function which fulfill the Kramers-Kronig relations. Even though good descriptions of the spectra are obtained, it turns out that the phonon self-energy effects can only partly be assigned to the redistributing background in this model. Linewidth anomalies, namely a sharpening in the underdoped, an intermediate broadening in the slightly overdoped, as well as strong softenings or hardenings in under- or overdoped samples remain. We conclude that these additional phonon self-energy effects indicate the presence of additional interactions and discuss possible explanations for their appearance.

II. THEORETICAL DESCRIPTION

As shown by Devereaux *et al.*¹² one can describe phonon Raman scattering via a correction of the electron-photon vertex $\gamma(\mathbf{k})$ plus additional terms arising from a photon-phonon vertex g_{pp} . The latter can be regarded as an abbreviation of the resonant excitation channel of the phonon involving interband excitations.¹⁵ In order to simplify the expression given for the mixed phononic and electronic response in Ref. 12, we neglect coupling to interband excitations in a first approximation. Figure 1 shows the Feynman diagram of the considered Raman process. When summing up the bubble diagrams one obtains the following expression for the full response function $\chi_\sigma(\omega)$ in symmetry channel σ of the lattice:

$$\chi_\sigma(\omega) = \gamma_\sigma^2 \chi_\sigma^e(\omega) - \gamma_\sigma^2 g_\sigma^2 \chi_\sigma^e(\omega)^2 D_\sigma(\omega), \quad (1)$$

where γ_σ represents the symmetry elements of the Raman vertex projected out by the incoming and outgoing polarization vectors and g_σ is the lowest order expansion coefficient of the electron-phonon vertex which is independent of momentum but may vary with temperature.¹² $\chi_\sigma^e(\omega) = R_\sigma^e(\omega) + i\rho_\sigma^e(\omega)$ is the electronic response, whose real and imaginary parts are connected by Kramers-Kronig relations, $D_\sigma(\omega) = D_\sigma^0(\omega)/[1 + g_\sigma^2 \chi_\sigma^e(\omega) D_\sigma^0(\omega)]$ is the renormalized, and $D^0(\omega) = 2\omega_p/(\omega^2 - \omega_p^2 + 2i\omega_p\Gamma)$ the bare phonon propagator. The latter contains the bare phonon frequency ω_p and the bare phonon linewidth Γ (HWHM). To simplify Eq. (1) further, we make the assumption that the phonon is only renormalized by the Raman-active electronic response $\gamma_\sigma^2 \chi_\sigma^e(\omega)$, neglecting all other self-energy contributions, e.g. those due to anharmonic phonon-phonon interactions. They are therefore included in ω_p and Γ .

The fluctuation-dissipation theorem relates the Raman intensity $I(\omega)$ to $[1 + n(\omega, T)] \text{Im} \chi_\sigma(\omega)$ with $n(\omega, T) = 1/[\exp(\hbar\omega/k_B T) - 1]$ the Bose factor. If A is the proportionality constant between the Raman efficiency $I_0(\omega) = I(\omega)/[1 + n(\omega, T)]$ and $\text{Im} \chi_\sigma(\omega)$ then the constant $C = A\gamma_\sigma^2/g_\sigma^2$ allows us to express the Raman efficiency in the following way:

$$I_0(\omega) = \varrho_*(\omega) + \frac{C}{\gamma(\omega) [1 + \epsilon^2(\omega)]} \times \left\{ \left[\frac{R_*(\omega)}{C} \right]^2 - 2\epsilon(\omega) \frac{R_*(\omega)}{C} \frac{\varrho_*(\omega)}{C} - \left[\frac{\varrho_*(\omega)}{C} \right]^2 \right\}, \quad (2)$$

with the substitutions $\varrho_*(\omega) = Cg_\sigma^2 \rho_\sigma^e(\omega)$, $R_*(\omega) = Cg_\sigma^2 R_\sigma^e(\omega)$, $\epsilon(\omega) = [\omega^2 - \omega_p^2(\omega)]/2\omega_p\gamma(\omega)$, $\gamma(\omega) = \Gamma + \varrho_*(\omega)/C$, and $\omega_p^2(\omega) = \omega_p^2 - 2\omega_p R_*(\omega)/C$.

It turns out that Eq. (2) is similar to the phenomenological Fano formula that Chen *et al.*¹³ obtained using an extended Green's function model, except that the phononic signal vanishes here when the electron-phonon coupling constant is zero. This is related to the fact that we have neglected the resonant excitation channel of the phonon so far. Therefore, one would expect a decreasing phonon intensity if the background decreases, or if the system becomes insulating. Examples for both cases are, e.g. the strong Fano-type profiles of the A_{1g} plane-oxygen phonons in $\text{HgBa}_2\text{Ca}_3\text{Cu}_4\text{O}_{10+\delta}$,¹ which almost vanish above T_c along with

the background feature, or the Fano-type Ba mode in xx or yy polarization in $\text{YBa}_2\text{Cu}_3\text{O}_{6+y}$ (Ref. 16) which is absent in the antiferromagnetic compound at $y=0$. In case of the here investigated B_{1g} phonon, however, it is known that substantial intensity is observed even at low oxygen contents.¹⁶ In order to connect Eq. (2) to the phenomenological Fano formula of Ref. 13 the replacement $R_*(\omega) \rightarrow R_*(\omega)+R_0$ in the numerator of the second term is sufficient. Hereafter we will refer to the modified equation as Eq. (2, R_0). The additional fit parameter $R_0 = Cg_\sigma^2 R_{pp}$ describes the intensity of the phonon originating from the resonant excitation channel.¹⁷ With this parameter one keeps a Lorentzian phonon at ω_p for vanishing effective electron-phonon coupling g_σ if $g_\sigma \cdot R_0$ remains finite. This replaces the $q^2 \cdot C_{Fano}$ -condition of simple Fano profiles where $I_{Fano}(\omega) = C_{Fano} \cdot (q + \epsilon)^2 / (1 + \epsilon^2)$ with $\epsilon = (\omega - \omega_\nu) / \gamma$ and q the asymmetry parameter.⁴ Physically that means that one obtains a Lorentzian profile with Eq. (2, R_0) when the phonon solely couples to electronic excitations which are strongly peaked away from the phonon energy. In reference to the simple Fano approach, in which the total phonon intensity is given by $I = \pi\gamma C_{Fano} q^2$,¹⁸ we find for the total and the bare phonon intensity $I_{tot} = \frac{\pi}{C} [R_*(\omega_p) + R_0]^2$ and $I_{phon} = \frac{\pi}{C} R_0^2$.

Our aim is to obtain the self-energy effects in a consistent way by using a phenomenological description of the electronic background. For this, we express the measured electronic response $\rho_*(\omega)$ with three terms:

$$\rho_*(\omega) = I_\infty \tanh(\omega/\omega_T) + \left[\frac{C_{2\Delta}}{1 + \epsilon_{2\Delta}^2(\omega)} - (\omega \rightarrow -\omega) \right] - \left[\frac{C_{sup}}{1 + \epsilon_{sup}^2(\omega)} - (\omega \rightarrow -\omega) \right]. \quad (3)$$

The first one describes the incoherent background,⁵ the second contribution models the 2Δ peak, and the third one the suppression of spectral weight seen at low Raman shifts. I_∞ , $C_{2\Delta}$, and C_{sup} are fit parameters for the respective intensities. Two-magnon excitations are not explicitly included in this description. The crossover frequency ω_T of the background, which is cut off at $\omega_{cut} = 8000 \text{ cm}^{-1}$, is used as a fit parameter, however, allowing only values close to the spot temperature. For the Lorentzians the abbreviations $\epsilon_j(\omega) = (\omega - \omega_j) / \Gamma_j$ with $j = 2\Delta, sup$ are used. The second terms in the brackets are necessary to fulfill the symmetry requirements for the Raman response. The Lorentzian modelling the suppression is arbitrarily bound to the other one by: $2\omega_{sup} = 2\Gamma_{sup} = \omega_{2\Delta} - \Gamma_{2\Delta}$ in order to reduce the number of free parameters. Eq. (3) is an appropriate way to model the imaginary part of the electronic response, however, the real part of the response function contains a constant error as a result of the arbitrarily chosen cut-off frequency.¹⁹ This error will modify the self-energy $R_*(\omega_p)/C$ and, as a consequence, the resonant intensity contribution R_0 . Both will hence depend on the chosen value of ω_{cut} . Analysis of the Ba mode in A_{1g} polarization confirms us that this error is small as this mode can almost completely be described by the interaction with the background independent of ω_{cut} .²⁰ In detail, it turns out that $R_*(\omega_p)/C \{R_0/C\}$ increases {decreases} by $I_\infty/C \cdot \frac{2}{\pi} \ln(\omega_{cut}^{new}/\omega_{cut}^{old})$ when the cutoff frequency is varied. With a typical value of $I_\infty/C = 1$ in the present study, corrections of $\sim 0.2 \text{ cm}^{-1}$ appear, when ω_{cut} is increased from 8000 cm^{-1} to 11000 cm^{-1} . Whereas the absolute values of the bare phonon frequency and the bare phonon intensity have to be considered with some care for the reason given above, the relative changes at different temperatures are not affected.

Even though all three terms in Eq. (3) are needed to describe the background below T_c , the last two terms diminish continuously close to the transition into the normal state. Above the transition, the background is almost entirely described by the incoherent contribution except for a small broad hump at the position where the 2Δ peak was observed close to T_c .

III. EXPERIMENTAL DETAILS

We study $Y_{1-x}(\text{Pr}, \text{Ca})_x\text{Ba}_2\text{Cu}_3\text{O}_7$ films with different doping levels achieved by substituting Y partially with Pr (underdoping) or Ca (overdoping). The investigated films are a $x=0.1$ Pr-doped film ($Y_{0.9}\text{Pr}_{0.1}$), a pure $x=0$ film (Y-123), and a $x=0.05$ Ca-doped film ($Y_{0.95}\text{Ca}_{0.05}$) abbreviated in the following as given in brackets. They have resistively measured T_c 's, as defined by zero resistance, of 86.3 K, 88.0 K, and 82.7 K, respectively. The films are grown by pulsed laser deposition on SrTiO_3 substrates in a process optimized to obtain high oxygen contents.²¹ Whereas the growth of the $Y_{1-x}\text{Pr}_x\text{Ba}_2\text{Cu}_3\text{O}_7$ films has also been optimized to obtain homogeneous and smooth films with low precipitate densities, the Ca-doped film exhibits a somewhat poorer surface quality, and a local variation of the Ca-content from the nominal value cannot be excluded. However, also for this film the temperature where the superconductivity-induced features vanish is in good agreement with the measured T_c . All films are c -axis oriented and their high degree of in-plane orientation allows us to study the plane-polarized excitation geometries.²¹ Raman spectra have been taken using the 458 nm Ar^+ line in a setup described elsewhere.²² They are corrected for the response of spectrometer and detector. We have used a power density of 110 Wcm^{-2} and an effective spot radius of $40 \mu\text{m}$ leading to a typical heating of 2 K in the laser spot.²³ All given temperatures are spot temperatures. In order to measure spectra with B_{1g} symmetry, the incident light was polarized along $x' = (1, 1, 0)$ and the scattered light along $y' = (1, -1, 0)$ in a coordinate system given by the crystal axes of the substrate.

IV. RESULTS

In Fig. 2 we show Raman spectra of the films below and above T_c . For a better comparison of the spectra we have normalized the intensity of the film Y-123 to unity above 650 cm^{-1} and used the same scaling factor for the other films as well. This factor is also used in the following figures. The spectra are efficiency corrected for the thermal factor $[1 + n(\omega, T)]$. The electronic continua, which are shown in the insets, are obtained after subtraction of the phonons. Whereas this can easily be done in case of the weak Ba and symmetric O(4) modes, the description given in Eq. (2, R_0) is used to subtract the B_{1g} mode properly. This description is also used for the O(4) mode in $Y_{0.9}\text{Pr}_{0.1}$ and for the Ba mode in $Y_{0.95}\text{Ca}_{0.05}$. In all films we observe a featureless background at 152 K which becomes almost constant above 400 cm^{-1} . At 18 K the B_{1g} 2Δ peaks are visible as well as suppressions of spectral weight at small Raman shifts. Whereas the B_{1g} 2Δ peak can clearly be seen in the raw data of $Y_{0.95}\text{Ca}_{0.05}$ they are somehow hidden in the spectra of the films with lower doping levels. In $Y_{0.9}\text{Pr}_{0.1}$ this results from the strongly reduced intensity of the redistribution (note the scale in the insets of Fig. 2) whereas in Y-123 it is a consequence of the destructive interference of phonon and background right at the position of the B_{1g} 2Δ peak. In agreement with recent

studies^{10,13} we find that the redistribution becomes weaker at low doping levels and that the B_{1g} 2Δ peak shifts with increasing doping to lower energies from 570 cm^{-1} in $Y_{0.9}Pr_{0.1}$ and 390 cm^{-1} in Y-123 down to 300 cm^{-1} in $Y_{0.95}Ca_{0.05}$. Compared to fully oxygenated single crystals the energy of the B_{1g} 2Δ peak in the film Y-123 is approximately 10 % lower.¹³ This indicates a higher doping level in the film compared to the single crystals. The increased doping level could result from additional oxygen which may enter the film at grain- or twin-boundaries. These boundaries appear with much higher densities in the films than in the single crystals as a result of the lattice mismatch to the substrate.

To give an example we show in Fig. 3(a) the efficiency $I_0(\omega)$ of the film $Y_{0.95}Ca_{0.05}$ measured at 18 K. Also shown is a fit to the spectrum where the B_{1g} phonon and the Ba mode are described according to Eq. (2), R_0 , and Lorentzians are taken for the O(4) mode and the weak feature around 600 cm^{-1} . Subtracting all phonons from the spectrum we obtain the electronic background $\varrho_*(\omega)$ which is shown in Fig. 3(b) together with the description according to Eq. (3) used in the fit. The real part of the electronic background $R_*(\omega)$ is shown in Fig. 3(c). In order to obtain $R_*(\omega)$ we have performed a numerical Hilbert transformation of $\varrho_*(\omega)$. For the transformation the measured spectrum is taken as constant for high frequencies up to ω_{cut} , and is interpolated to zero intensity at $\omega = 0$; for negative frequencies the antisymmetry of $\varrho_*(\omega)$ has been used. Whereas a good description of the spectrum can also be obtained with a simpler model where the real part of the response function is considered constant,¹³ our approach simultaneously yields a good description of $R_*(\omega)$ which is important when phonon self-energy effects are investigated. The temperature dependencies of the B_{1g} 2Δ peaks $\omega_{2\Delta}$ of the films are shown in the inset of Fig. 3 where a typical phonon frequency is indicated as a dashed horizontal line. Whereas the peak is always below the phonon frequency in the Ca-doped film it is always above the phonon in the Pr-doped film. In the film Y-123 the peak passes the phonon around 60 K. In all films only weak temperature dependencies are observed in agreement with other Raman studies.²⁴ With increasing temperature the intensities of the background peaks decrease, becoming unresolvable above T_c .

The temperature dependencies of the fit parameters of the B_{1g} phonons are shown in Fig. 4. Beside the bare phonon parameters and the self-energy contributions at $\omega = \omega_p$ also the renormalized frequencies $\omega_\nu(\omega_p)$ and linewidths $\gamma(\omega_p)$ are depicted which facilitates a comparison with previous data obtained with simpler Fano models. Solid lines are fits to the anharmonic decay for both models,¹⁸ and anomalies below T_c are discussed with respect to these fits. Looking at the renormalized phonon parameters, we observe a behavior which is in agreement with the relative positions of B_{1g} 2Δ peak and phonon energy: We find a softening in $Y_{0.9}Pr_{0.1}$ and Y-123 where $\omega_{2\Delta}(T \rightarrow 0) > \omega_p$ and a hardening in $Y_{0.95}Ca_{0.05}$ where $\omega_{2\Delta}(T \rightarrow 0) < \omega_p$ (see Fig. 3). In those two films where the B_{1g} 2Δ peaks evolve in the vicinity of the phonon we find strong broadenings of $\approx 5 \text{ cm}^{-1}$ whereas a sharpening of $\approx 2 \text{ cm}^{-1}$ occurs in $Y_{0.9}Pr_{0.1}$. Our fit procedure now allows us to identify the self-energy effects which originate from the background. For all films a convincing correlation exists between the changes of the linewidth appearing below T_c and the varying self-energy contributions $\varrho_*(\omega_p)/C$. It turns out that the sharpening in $Y_{0.9}Pr_{0.1}$ is a consequence of a reduced effective coupling $g_{B_{1g}}^2 \propto 1/C$ at low temperatures, as the background intensity at the phonon position $\varrho_*(\omega_p)$ varies hardly with temperature (see Fig. 2). The broadenings of the other films on the other hand are almost entirely described by increasing intensities

$\varrho_*(\omega_p)$ accompanied by increasing effective couplings. However, looking at the bare phonon linewidths Γ some anomalies remain, i.e. a slight sharpening of $\approx 1.5 \text{ cm}^{-1}$ and a slight broadening of $\approx 1 \text{ cm}^{-1}$ in $\text{Y}_{0.9}\text{Pr}_{0.1}$ and $\text{Y}_{0.95}\text{Ca}_{0.05}$, respectively, as well as an intermediate broadening of $\approx 1.5 \text{ cm}^{-1}$ in Y-123 appearing around 60 K. Regarding the frequency effects even stronger anomalies are observed. Whereas we find a good explanation of the softening in Y-123 as a result of the varying contribution $R_*(\omega_p)/C$, the bare phonon frequencies ω_p in the other films differ significantly from an anharmonic behavior, showing pronounced softening or hardening in $\text{Y}_{0.9}\text{Pr}_{0.1}$ or $\text{Y}_{0.95}\text{Ca}_{0.05}$, respectively. The appearance of such an anomaly in the Pr-doped film is related to the fact that only a small redistribution is observed, the anomaly in the Ca-doped film, however, is unexpected.

Finally, we turn to the lowest row of Fig. 4 in which beside the total intensities I_{tot} also the bare phonon intensities I_{phon} are given. Even though increasing intensities are observed below T_c in both films which exhibit B_{1g} 2Δ peaks above the phonon energy, they have different origins. Whereas the increase in $\text{Y}_{0.9}\text{Pr}_{0.1}$ can be assigned to the increasing values of R_0 which compensate the decreasing effective coupling, they are a result of an increasing background contribution $R_*(\omega_p)$ accompanied by an increasing effective coupling in the film Y-123. No intensity anomaly is observed in the film $\text{Y}_{0.95}\text{Ca}_{0.05}$ where independent of the temperature the B_{1g} 2Δ peak is below the phonon energy. A superconductivity-induced increase of the interband contribution to the Raman intensity of the B_{1g} phonon has been obtained in a theoretical treatment of the scattering process by Sherman *et al.*²⁵ The latter authors showed that the increase will depend on the doping level, becoming stronger in underdoped samples. This appears to be in agreement with our data. Our results, however, also indicate that there is a particular correlation between the intensity anomaly due to the interband contribution R_0 and the relative energies of phonon and B_{1g} 2Δ peak which has not been observed before. A further discussion of this correlation will be presented in a forthcoming publication.²⁶

V. DISCUSSION AND CONCLUSIONS

The remaining anomalies of the bare phonon parameters show that additional interaction effects are present which modify Eqs. (1) and (2, R_0). In the following we will discuss two possible origins of the observed anomalies: (i) The assumption that the phonon interacts with the entire measured background is wrong; (ii) An additional excitation exists which renormalizes the phonon but is not Raman-active.

(i): If the electronic continuum consists of several contributions interacting only partly with the phonon, the applied fitting procedure would not allow us to obtain the proper bare phonon parameters. In fact, in the antiferromagnetic phase $\text{YBa}_2\text{Cu}_3\text{O}_6$, in which intra-band excitations have vanished, one still observes a background on which the B_{1g} phonon is superimposed.¹⁶ The symmetric appearance of the phonon indicates the absence of coupling to that background, which can more or less unambiguously be related to two-magnon scattering.^{27,28} At higher doping levels the two-magnon intensity decreases.^{29,30} However, in previous works we have shown that in low up to slightly overdoped superconducting $\text{Y}_{1-x}\text{Pr}_x\text{Ba}_2\text{Cu}_3\text{O}_7$ (Ref. 31) and $\text{Bi}_2\text{Sr}_2\text{CaCu}_2\text{O}_{8+\delta}$ (Ref. 32) compounds the magnetic scattering in B_{1g} symmetry becomes amplified below T_c having significant spectral weight at low frequencies. The observation that the effective coupling decreases below T_c in $\text{Y}_{0.9}\text{Pr}_{0.1}$

is thus in agreement with a strengthening of magnetic excitations in that temperature range. However, studying $\text{Bi}_2\text{Sr}_2\text{CaCu}_2\text{O}_{8+\delta}$ single crystals³³ we have seen recently that the superconductivity-induced changes at high energy transfers vanish at very high doping levels. Therefore, the influence of the magnetic scattering should decrease with increasing doping. The similar strength of the anomalies in the overdoped film $\text{Y}_{0.95}\text{Ca}_{0.05}$ can thus not be related to the existence of magnetic excitations which presumably are strongly overdamped at this doping level. Therefore, our observation might have a different origin at higher doping levels.

(ii): In the second scenario anomalies in the underdoped as well as in the overdoped regime can be explained by assuming the presence of an additional not Raman-active excitation. The energy of this excitation must be strongly related to the gap value in order to explain the intermediate broadening in Y-123 which appears in the temperature range where the measured B_{1g} 2Δ peak passes the phonon frequency. In fact, the doping dependence of such a broadening in several $\text{YBa}_2\text{Cu}_3\text{O}_{7-\delta}$ single crystals with different oxygen contents³⁴ agrees well with the doping dependence of the B_{1g} 2Δ peak obtained on the same crystals.¹³ The intermediate broadening cannot be attributed to the Raman-active gap excitations as $\rho_*(\omega_p)/C$ shows a monotonic behavior at the considered temperatures within the error bars. The small temperature interval of the broadening indicates that the imaginary part of the response function associated with this excitation has a small extension in frequency space of roughly $\pm 20 \text{ cm}^{-1}$ as $\omega_{2\Delta}$ varies only slightly below T_c . 2Δ peaks of this sharpness have indeed not been observed in Raman spectra of cuprates so far. Even though the imaginary part of the response function has a rather small width, the real part will extend to a somewhat broader frequency range and could therefore be responsible for the anomalous softenings and hardenings in $\text{Y}_{0.9}\text{Pr}_{0.1}$ and $\text{Y}_{0.95}\text{Ca}_{0.05}$. In this picture the almost anharmonic behavior of the bare phonon frequency in Y-123 is not surprising as the real part changes sign when the gap passes the phonon.

The origin of the additional excitation which renormalizes the phonon but does not show up in the Raman spectra could possibly be found in a not Raman-active gap excitation. As seen before¹⁰ and shown in this work the gap features rapidly lose their strength at lower doping levels. This cannot be understood on the basis of the standard theory³⁵ where a metal-like band picture is used to describe the response in the superconducting state. It has therefore been suggested that vertex corrections due to the strong correlations should be considered in order to understand the additional screening which suppresses the gap features in the Raman process.^{9,33} This work provides some evidence that screening of the B_{1g} Raman response may not only be present around or below the optimum doping level where the cuprates may be regarded as doped antiferromagnets, but also above this level when the cuprates start to evolve into a metallic state.

In conclusion, we present a model that allows us to study background redistributions and related phonon self-energy effects in $\text{Y}_{1-x}(\text{Pr}, \text{Ca})_x\text{Ba}_2\text{Cu}_3\text{O}_7$ films simultaneously. In this model we use a phenomenological description of the electronic background and find that this approach enables us to explain various self-energy effects. However, some anomalies remain. We discuss whether these anomalies result from the fact that the observed background consists in a subtle way of electronic as well as magnetic excitations, or whether they also indicate that another not Raman-active excitation, which we suggest to originate from the gap itself, renormalizes the phonon.

ACKNOWLEDGMENTS

The authors thank M. Käll, M.V. Klein, D. Manske and U. Merkt for stimulating discussions. S.O., C.T.R., and M.R. acknowledge grants of the German Science Foundation via the Graduiertenkolleg “Physik nanostrukturierter Festkörper”.

REFERENCES

- * Present Address: Condensed Matter Physics, Chalmers University of Technology, 41296 Göteborg, Sweden.
- ¹ V.G. Hadjiev, Xingjiang Zhou, T. Strohm, M. Cardona, Q.M. Lin, and C.W. Chu, Phys. Rev. B **58**, 1043 (1998).
- ² D. Reznik, B. Keimer, F. Dogan, and I.A. Aksay, Phys. Rev. Lett. **75**, 2396 (1995).
- ³ B. Friedl, C. Thomsen, and M. Cardona, Phys. Rev. Lett. **65**, 915 (1990).
- ⁴ S.L. Cooper and M.V. Klein, Comments Cond. Mat. Phys. **15**, 99 (1990).
- ⁵ C.M. Varma, P.B. Littlewood, S. Schmitt-Rink, E. Abrahams, and A.E. Ruckenstein, Phys. Rev. Lett. **63**, 1996 (1989).
- ⁶ T.P. Devereaux, D. Einzel, B. Stadlober, R. Hackl, D.H. Leach, and J.J. Neumeier, Phys. Rev. Lett. **72**, 396 (1994).
- ⁷ C. Jiang and J.P. Carbotte, Phys. Rev. B **53**, 11 868 (1996).
- ⁸ T. Strohm and M. Cardona, Phys. Rev. B **55**, 12 725 (1997).
- ⁹ D. Manske, A. Bock, C.T. Rieck, and D. Fay, Phys. Rev. B **58**, 8841 (1998); Reply to T. Strohm, D. Munzar, and M. Cardona, Phys. Rev. B **58**, 8839 (1998).
- ¹⁰ R. Nemetschek, M. Opel, C. Hoffmann, P.F. Müller, R. Hackl, H. Berger, L. Forró, A. Erb, and E. Walker, Phys. Rev. Lett. **78**, 4837 (1997).
- ¹¹ J.M. Harris, Z.-X. Shen, P.J. White, D.S. Marshall, M.C. Schabel, J.N. Eckstein, and I. Bozovic, Phys. Rev. B **54**, R15 665 (1996).
- ¹² T.P. Devereaux, A. Virosztek, and A. Zawadowski, Phys. Rev. B **51**, 505 (1995).
- ¹³ X.K. Chen, E. Altendorf, J.C. Irwin, R. Liang, and W.N. Hardy, Phys. Rev. B **48**, 10 530 (1993).
- ¹⁴ E.T. Heyen, S.N. Rashkeev, I.I. Mazin, O.K. Andersen, R. Liu, M. Cardona, and O. Jepsen, Phys. Rev. Lett. **65**, 3048 (1990).
- ¹⁵ W. Hayes and R. Loudon, *Scattering of Light by Crystals* (John Wiley & Sons, New York 1978).
- ¹⁶ G. Burns, F.H. Dacol, C. Feild, and F. Holtzberg, Physica C **181**, 37 (1991).
- ¹⁷ Comparing Eq. (2, R_0) with the microscopic and phenomenological results given in Eq. (32) of Ref. 12 and in Eq. (6) of Ref. 13, respectively, one finds $R_{pp} = g_{pp}/(g_\sigma \cdot \gamma_\sigma)$ and $R_{pp} = T_p/(V \cdot T_e)$, where T_p and T_e are transition matrix elements for phononic and electronic excitations and V is the coupling between both excitations.
- ¹⁸ see, e.g. Ref. 1 and references therein.
- ¹⁹ The Hilbert transformed incoherent contribution is:

$$R_{inc}(\omega) = I_\infty \left[0.5 + \frac{2}{\pi} \ln(\omega_{cut}/\omega_T) + \sqrt{2} \operatorname{artanh}(p - 1) \right], \text{ with } p = \tanh(\omega/\omega_T)/(\omega/\omega_T).$$
- ²⁰ A. Bock, S. Ostertun, and K.-O. Subke, unpublished.
- ²¹ N. Dieckmann, M. Rübhausen, A. Bock, M. Schilling, K.-O. Subke, U. Merkt, E. Holzinger-Schweiger, Physica C **272**, 269 (1996).
- ²² A. Bock, R. Das Sharma, S. Ostertun, and K.-O. Subke, J. Phys. Chem. Solids **59**, 1954 (1998).
- ²³ A. Bock, Phys. Rev. B **51**, 15 506 (1995).
- ²⁴ M. Boekholt, M. Hoffmann, and G. Güntherodt, Physica C **175**, 127 (1991).
- ²⁵ E.Ya. Sherman, R. Li, and R. Feile, Phys. Rev. B **52**, R15 757 (1995).
- ²⁶ A. Bock, unpublished.

- ²⁷ K.B. Lyons, P.A. Fleury, L.F. Schneemeyer, and J.V. Waszczak, Phys. Rev. Lett. **60**, 732 (1988).
- ²⁸ P. Knoll, C. Thomsen, M. Cardona, and P. Murugaraj, Phys. Rev. B **42**, 4842 (1990).
- ²⁹ G. Blumberg, R. Liu, M.V. Klein, W.C. Lee, D.M. Ginsberg, C. Gu, B.W. Veal, and B. Dabrowski, Phys. Rev. B **49**, 13 295 (1994).
- ³⁰ G. Blumberg, Moonsoo Kang, M.V. Klein, K. Kadowaki, and C. Kenziora, Science **276**, 1427 (1997).
- ³¹ M. Rübhausen, C.T. Rieck, N. Dieckmann, A. Bock, and U. Merkt, Phys. Rev. B **56**, 14 797 (1997).
- ³² M. Rübhausen, P. Guptasarma, D.G. Hinks, and M.V. Klein, Phys. Rev. B **58**, 3462 (1998).
- ³³ M. Rübhausen, PhD thesis (Shaker Verlag, Aachen 1999).
- ³⁴ E. Altendorf, X.K. Chen, J.C. Irwin, R. Liang, and W.N. Hardy, Phys. Rev. B **47**, 8140 (1993).
- ³⁵ M.V. Klein and S.B. Dierker, Phys. Rev. B **29**, 4976 (1984).

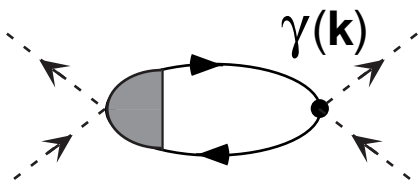
FIGURES

FIG. 1. Feynman diagram for phononic Raman scattering, where $\gamma(\mathbf{k})$ and $g(\mathbf{k})$ are the electron-photon and electron-phonon vertices, and solid and wavy lines the electron and phonon propagator. The outer dashed lines correspond to the photons.

FIG. 2. Raman efficiencies in B_{1g} symmetry of the three investigated films at $T = 18$ K (solid lines) and 152 K (dots). The insets show the electronic backgrounds after subtraction of the phonons. The efficiencies are given in the same units.

FIG. 3. (a) Raman efficiency $I_0(\omega)$ in B_{1g} symmetry of the film $Y_{0.95}Ca_{0.05}$ at $T = 18$ K (open circles), and fit result (solid line). (b) Imaginary part $\varrho_*(\omega)$ and (c) numerically determined real part $R_*(\omega)$ of the electronic background (open circles) obtained after subtraction of the phonons, and numerical descriptions used in the fit (solid lines). Efficiencies and real part are given in the same units. Arrows indicate the energy of the 2Δ peak given by the fit parameter $\omega_{2\Delta}$. The inset shows the energies $\omega_{2\Delta}$ versus temperature for the three investigated films as indicated. The horizontal dashed line represents a typical energy of the B_{1g} phonon of 345 cm^{-1} .

FIG. 4. Temperature dependence of the fit parameters for the B_{1g} phonon. Closed circles represent the bare phonon parameters ω_p , Γ , and I_{phon} , crosses the self-energy contributions $R_*(\omega_p)/C$ and $\varrho_*(\omega_p)/C$, and open circles the calculated renormalized values $\omega_\nu(\omega_p)$, $\gamma(\omega_p)$, and I_{tot} . Solid lines are fits according to an anharmonic decay. The vertical dotted lines indicate the respective transition temperatures of the films. Marker sizes represent the vertical accuracies.



with:



=



+

